Experimental investigation of in-plane loaded timber-framed rammed earth panels. Part I: monotonic shear-compression tests

Riccardo Barsotti[1], Stefano Bennati[2], Daniel V. Oliveira[3]

[1] Corresponding author, email riccardo.barsotti@unipi.it, Department of Civil and Industrial Engineering, University of Pisa, 56122 Pisa, Italy
[2] Department of Civil and Industrial Engineering, University of Pisa, 56122 Pisa, Italy
[3] Department of Civil Engineering, ISISE University of Minho, Azurém, 4800-058 Guimarães, Portugal

Abstract
Rammed earth walls show comparatively good performances with respect to vertical loads, while their stiffness and strength against horizontal loads are often unsatisfactory. Preliminary indications about the timber-framed rammed earth panel (TREP) stiffness and load bearing capacity have been obtained from a first experimental study that has been expressively set up and performed to investigate the TREP in-plane static behavior. The present part I, together with the subsequent part II (companion paper), illustrates and discusses the key experimental results obtained from the compression-shear loading tests performed on rammed earth panels reinforced by a contouring timber frame. In the present part I of the paper, the monotonic loading tests are carefully analyzed, the results are discussed, and the detected damage modes are explained. The results seem to show that the reinforcing timber frame provides a substantial benefit enabling the development of an effective "strut-and-tie" resisting mechanism that effectively exploits the compressive strength of the rammed earth panel and promotes a ductile failure mode.

1. Introduction
Earth has been used as a building material since the earliest times in history: as an example, mud brick (adobe) dating from 8000 to 6000 BC have been found in central Asia and in the Middle East [1]. Crossing the centuries, construction of rammed earth buildings has continued into modern times as well, although mostly in less developed countries. Earth materials have been quickly replaced by masonry and wood; moreover, since the 19th century, new and more advanced building materials, such as concrete and steel, became available due to the acceleration impressed on technology along with the industrial development, and more technologically developed countries, particularly in Europe, began to use increasing amounts of these advanced building materials.
Nowadays, materials such as concrete and steel are extensively used in civil engineering because of their high strength/density and stiffness/density ratios and their relatively low unit cost. On the other hand, these materials are energy consuming and devour large amounts of natural resources. The growing concern, especially in recent years, about embodied energy and climate change has renewed the interest for more sustainable building processes and materials that could be effectively used in combatting climate change by reducing the world's greenhouse gas emissions. In this context, traditional building materials, such as raw earth, are re-garnering interest, also because of their recyclability.
The present paper aims at improving the sustainability of building constructions by exploiting the use of "*rammed earth*" structural elements, that is, elements made of earth material compacted within a formwork. Rammed earth panels exhibit good mechanical responses when they are subjected to vertical loads, while their strength and stiffness against horizontal actions are comparatively low. In this regard, a countermeasure adopted since ancient times in seismic regions consists in suitably combining rammed earth panels with timber elements or vegetal fibers. Timber elements have long been used

to endow rammed earth structural elements with some tensile strength [2]. Many different examples of this kind of structures can be found all around the world, all of which are usually referred to in modern literature as Timber-Framed Masonry (TFM). A very clear map showing the TFM world distribution can be found in [3].
The present contribution is the first of a two-part paper presenting and discussing experimental results obtained from monotonic and cyclic compression-shear loading tests performed on rammed earth panels reinforced by a contouring timber frame. The present part I deals with the monotonic loading tests and it is organized as follows. Section 2 describes the Timber-Framed Rammed Earth Panel (TREP) that has been designed and built specifically for the test. Section 3 addresses the experimental setup and the two compression-shear monotonic loading tests. The main results obtained from the tests are shown and discussed in Section 4, while a detailed survey of the damage in the panel and in timber frame is provided in Section 5. The cyclic loading tests are addressed in a companion paper (part II) [4].

2. A low-cost fully recyclable structural element for earth buildings

The assessment of the mechanical response of rammed earth walls, subjected to in-plane and out-of-plane loads, is the subject of a growing interest in recent years among the researchers working in the field of the mechanics of structures. Here, without any claim to completeness, it's recalled that the issues of determining the stiffness and load capacity of stabilized and unstabilized rammed earth walls are addressed by way of example in [5 – 9]; some study cases concerning rammed earth walls strengthened with bonded fibers are illustrated in [10 - 11].
All the studies agree that rammed earth walls show comparatively good performances with respect to vertical loads, while their stiffness and strength against horizontal loads are in many cases unsatisfactory [12], [13]. In order to provide rammed earth panels with some additional strength and stiffness against horizontal actions, this paper focused on the design of a panel reinforced by a contouring timber frame. As stated above, the general idea is all but new. Timber is one of the oldest structural materials [14] [15], and its use combined with masonry or earth materials is testified by the many examples that can be found in different parts of the world and that can be traced back to different ages [16], [17] (Figure 1).

a)  *b*) 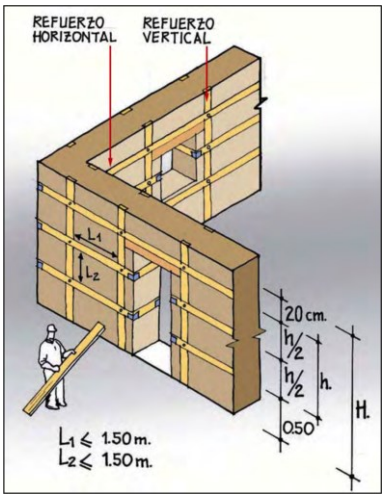

Figure 1: *a*) Hımış building in Anatolia with mud-brick and timber frames [18]; *b*) timber reinforcement of adobe or pisé constructions proposed by AIS Colombia [19].

2.1 Geometry of TREP elements

Four TREP elements have been built for the test, all sharing the same geometry. As shown in Figure 2, each TREP consists of a 25 cm thick rammed earth square panel whose side is 150 cm long, surrounded by a glue-laminated timber (GL24h) frame composed of two vertical columns with 16x16 cm^2 cross-section and two horizontal beams with 32x16 cm^2 cross-section. In order that good contact conditions could be assured between the timber frame and earth panel, a 25x150 cm^2 timber board 2 cm thick is nailed at the internal side of each column. A 16x16 cm^2 hole with corners slightly rounded is drilled at both the ends of each horizontal beam. At both the columns top and bottom end, the corners have been slightly rounded to ease plugging them into the beam holes. Each column-beam connection is provided with four M12 bolts class 8.8 with a gross length of 360 mm.

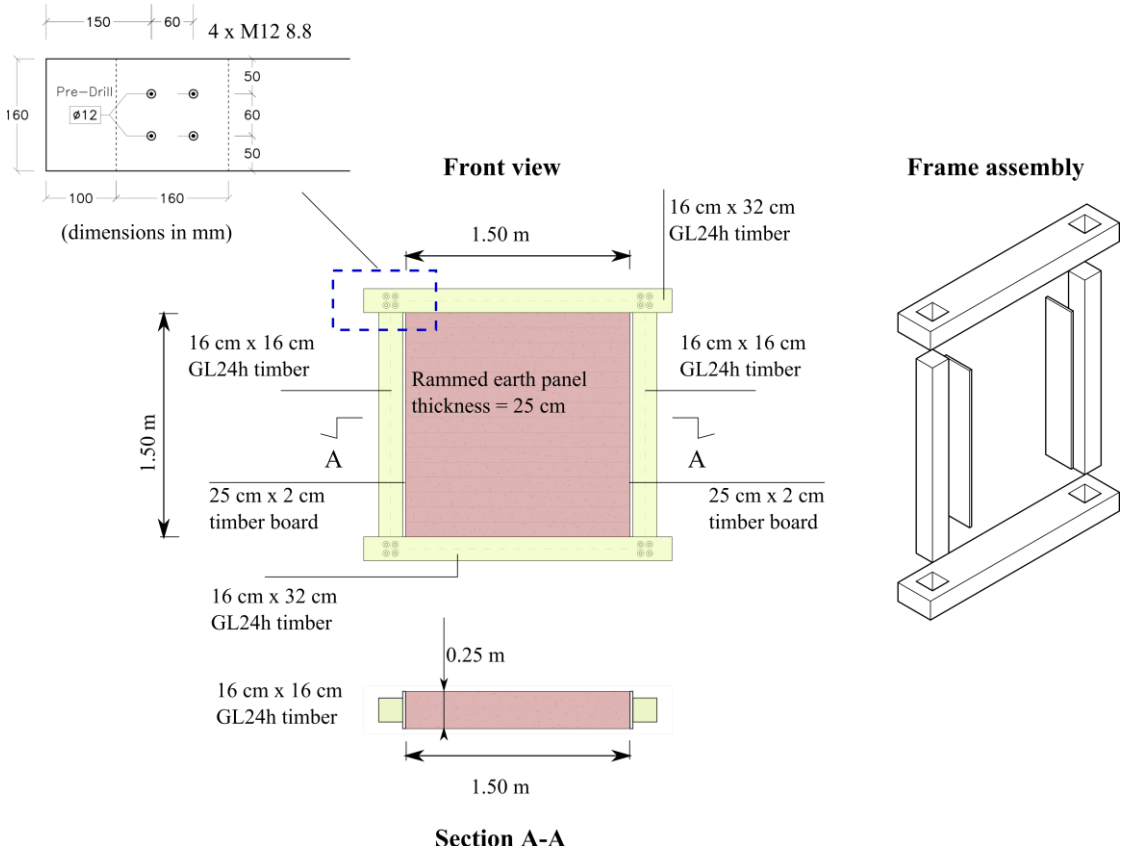

Figure 2: shape and dimensions of the TREP element.

The TREP elements that have been built for the test were thought as half-scale prototypes of a bearing element that could be embedded in actual building walls. As it will be illustrated more in detail in the following, before the test a mean vertical compressive stress of 0.13 MPa has been imposed on the element, which is a stress level of the same order as that in a two-storey residential building.

Assemblage of the TREP elements and execution of the experimental tests were carried out at the Department of Civil Engineering of the University of Minho, Guimarães, Portugal.

2.2 Assembling of the TREP elements and TF frames

The assembly of the TREP elements proceeded accordingly to the following sequential phases, see also Figure 3:

a) The foot of the columns is inserted into the bottom beam (I – II).
b) The holes that host the bolts at each beam-column joint are drilled to minimize the clearance. The bolts at the bottom of the column are fastened; two timber boards of 2 cm thick are nailed at the internal side of each column (III – V).
c) The rammed earth panel is progressively built. Each earth layer has an initial thickness of 15 cm and is manually compacted by a given number of rammer blows dropped from a predetermined height (VI – VII).
d) The top beam is put in place without locking it to the columns of the wooden frame (VIII). As it will be explained later, by this way the top beam can slide down the columns and this ~~has been done to~~ enable introducing an initial compressive stress field in the rammed earth panel during the initial stage of preparation of the test. The compressive preload is expected to have a beneficial effect on the structural response, as well documented in the literature (see, for example [20]).
e) The panel was left drying for a suitable period, not less than two months.
f) Before carrying out the test, the small detachments (up to 5 mm) at the interface between the panel and the timber elements due to shrinkage of the rammed earth were sealed using an earth mortar. The earth in the mortar was the same as in the panel. To ensure continuity of contact over the entire interface, a grout composed of kaolinite and limestone powder was injected to promote full contact between the rammed earth panel and the timber boards.
g) At the beginning of the loading test, after completing of the preload phase, the upper beam is connected to the columns, by inserting and tightening the bolts.

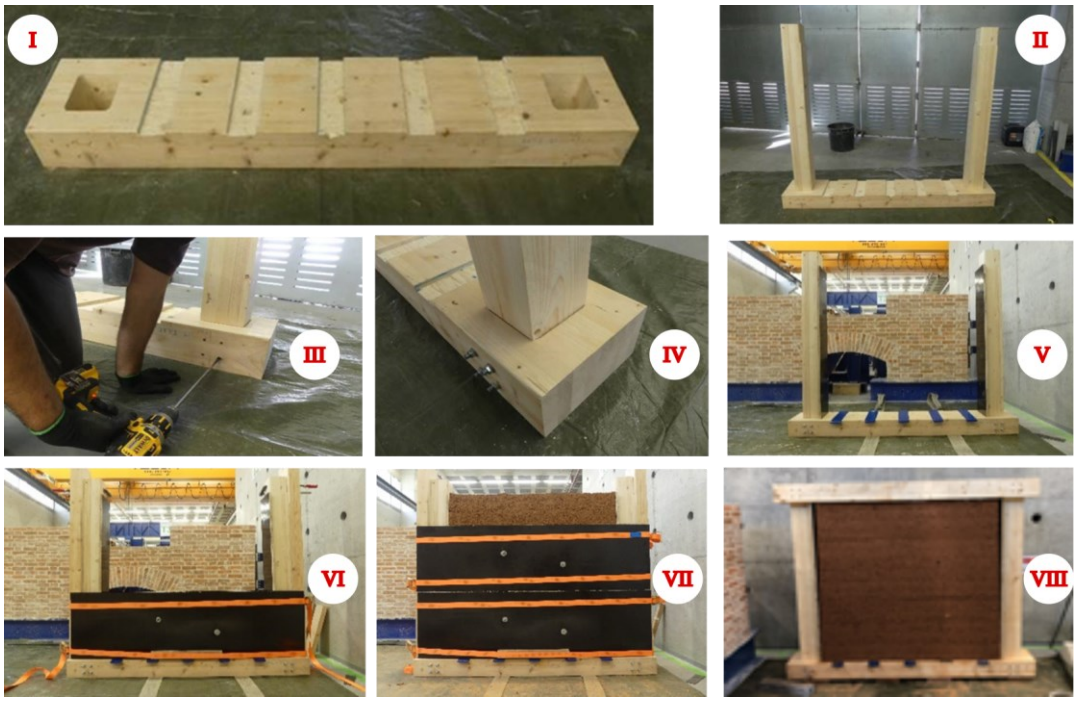

Figure 3: Assembly phases of the TREP element.

The experimental campaign also involved the construction of three bare timber frames, named TF. The TFs were readily built by the simultaneous assembly of beams and columns. The timber elements were connected by the same bolted joints as in the TREP elements. Unreinforced rammed earth panels are going to be built in the next step of the research for comparison purposes.

2.3 Mechanical properties of the materials

The timber frame is made of GL24h glue-laminated elements according to EN 14080:2013, provided by a local company (Table 1). The timber density and compressive strength have also been checked experimentally by the authors only to the aim of confirming the glulam strength class declared by the manufacturer ~~and are reported in Table 1~~. The earth panel is built with clayey soil provided by a Portuguese contractor mixed with gravel and sand coming from quarries nearby the Minho region (north Portugal) so as to modify the particle size distribution and make it fall within the acceptable range (envelope introduced in [21]), see Figure 4. The mean initial water content in the earth layers is estimated between 10 % and 11 %. Experimentally assessed physical and mechanical main properties of soil are summarized in Table 2. The compressive strength and elastic modulus of the rammed earth material have been determined from compressive tests performed on six cylindrical specimens with a height/diameter ratio of 2 to 1, a commonly accepted standard (see, for example [5], [8]). It is worth observing that the values of the compressive strength and elastic modulus of the earth material are in good agreement with those documented in [5].

Property	Value
Compressive strength*	31 ± 4 (13 %) MPa
Tensile strength	19,2 MPa
Shear strength	3,5 MPa
Density*	408 ± 54 (13 %) kg/m^3

Table 1: Mechanical and physical properties of glulam timber (* = directly tested; coefficient of variation is given inside parenthesis).

Property		Value
Compressive strength		0.51 ± 0.03 (6%) MPa
Elastic modulus		96 ± 23 (24%) MPa
Granulometric Fraction	Clay	10 %
	Lime	11 %
	Sand	33 %
	Gravel	46 %
Atterberg limits	Liquid Limit	25 %
	Plastic Limit	21 %
	Shrinkage Limit	4 %
Optimum Water Content	OWC	11.1 %
	γ_{OWC}	2.02 g/cm^3

Table 2: Mechanical and physical properties of soil (coefficient of variation is given inside parenthesis).

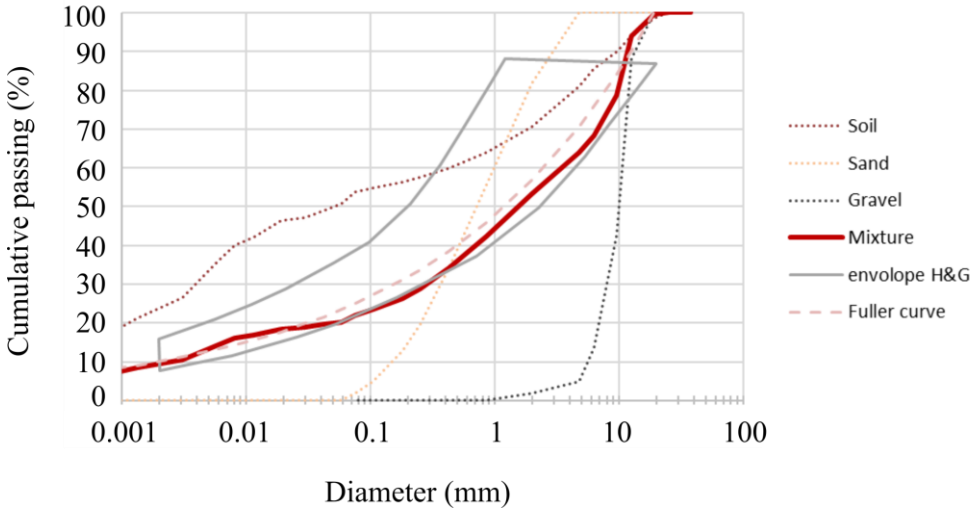

Figure 4: Particle size distribution used for the TREP elements (the envelope indicated in [21] and the Fuller curve are also displayed).

3. Experimental campaign

In the literature, no theoretical models or experimental results are available on the mechanical response of innovative elements such as the TREP element proposed here. Hence, to obtain some preliminary indications about their stiffness and load bearing capacity, a first set of experimental study has been expressively set up and performed.
The experiments focused on the TREP in-plane static behavior under shear-compression loading conditions. A total of four rammed earth panels reinforced with timber elements (TREP1, TREP2, TREP3 and TREP4) along with three timber frames without earth filling (TF1, TF2 and TF3) were built for the tests. Two TREP elements have been tested until collapse by monotonically increasing the horizontal load, while the other two elements have been tested under cyclic loading conditions. The three bare timber frames have also been tested under shear loading condition to better highlight the coupling effect between timber and earth.
The test program was composed of:

- two monotonic shear load tests carried out on the bare timber frames TF1 and TF2; the horizontal load was imposed under monotonic displacement control.
- two monotonic shear-compression load tests carried out on TREP1 and TREP2 elements; the vertical load was kept constant while the horizontal load was imposed under monotonic displacement control.
- one cyclic shear load test carried out on the TF3 timber frame; the horizontal load was imposed under cyclic displacement control.
- two cyclic shear-compression load tests carried out on TREP3 and TREP4 elements; the vertical load was kept constant whereas the horizontal load was imposed under cyclic displacement control.

The present part I of the paper addresses the monotonic loading tests (TF1, TF2, TREP1 and TREP2 elements) while the cyclic tests (TF3, TREP3 and TREP4) are addressed in part II [4]. The in-plane shear-compression tests constitute the first part of a wider experimental program which will be extended to the investigation of the out-of-plane behavior of TREP elements in the next further steps of the research.

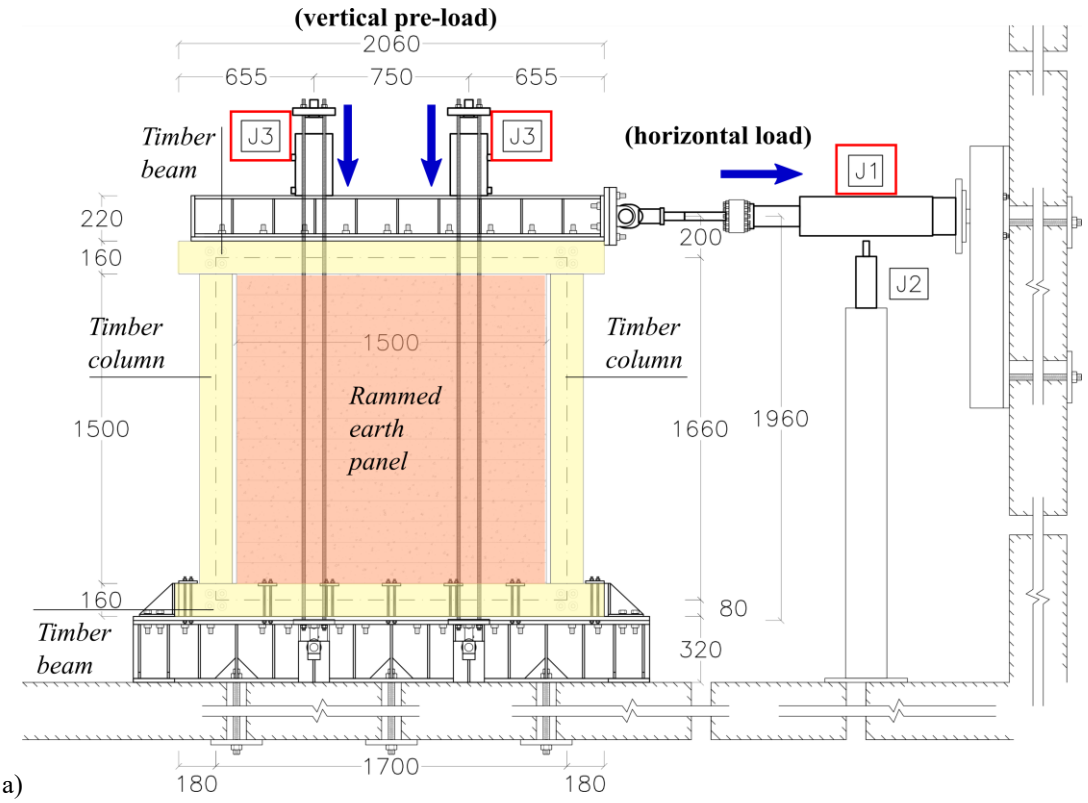

a)

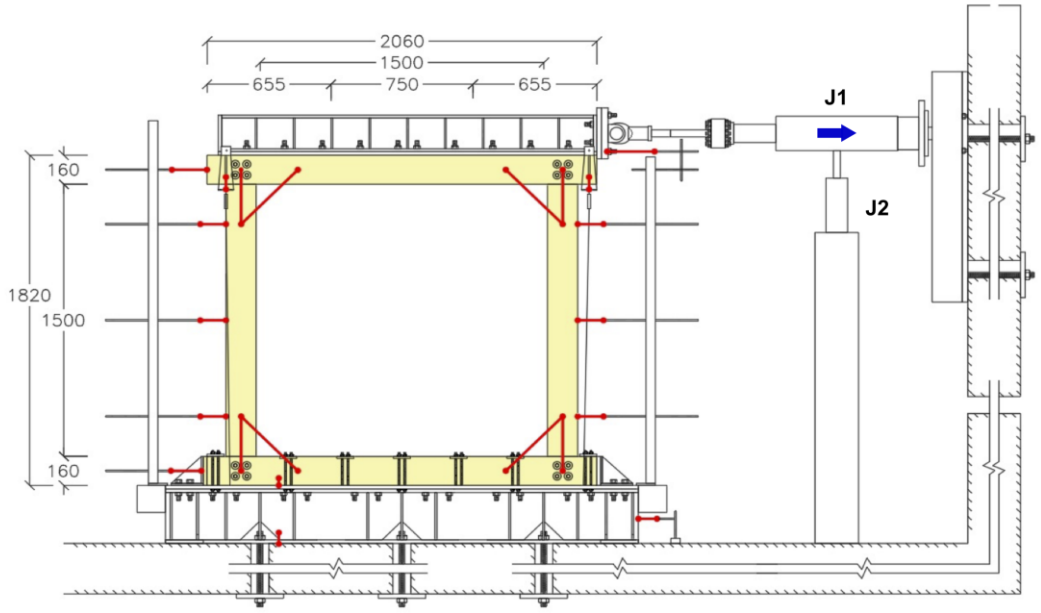

b)

Figure 5: in-plane shear-compression test setup (all dimensions in mm):
a) TREP elements; b) TF timber frames.

In the two in-plane monotonic shear-compression tests the vertical load has been kept constant while a progressively increasing horizontal displacement has been applied to the TREP element. The test set-up is graphically illustrated in Figure 5a. The horizontal load is imposed by the "J1" jack having a capacity of 300 kN and a range of ± 200 mm. The test is carried out by progressively increasing the displacement of the jack head at a constant speed of 0.05 mm/s.

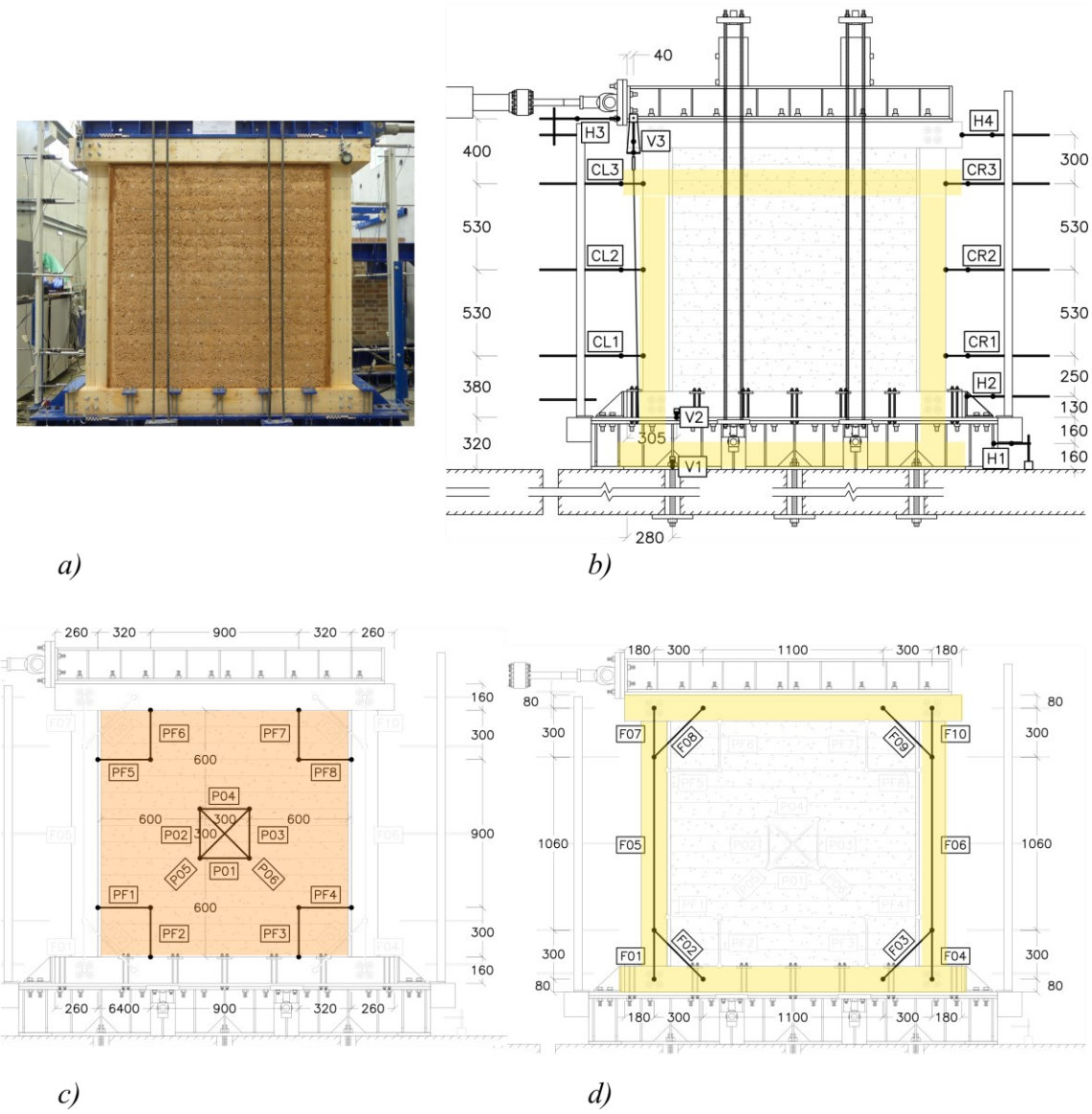

Figure 6: LVDT arrangement: *a*) overall view of the TREP1 test instrumentation; *b*) LVDT on the lateral side of the timber columns; *c*) LVDT on the rear face at the center of the panel and at the frame-panel interface; *d*) LVDT on the front of timber elements (dimensions in mm).

A compressed air piston "J2" is placed below jack J1 to keep it horizontal. A constant vertical load of 50 kN is applied to the upper steel beam by means of two manually controlled jacks labelled "J3". Each vertical jack contrasts on four high-strength, 16 mm diameter steel bars, in turn constrained at their foot to a rigid steel beam located at the panel base. Each vertical jack is equipped with a load cell; during the test, the vertical load was kept approximately constant by checking the value provided by the load cells.
The vertical load is aimed at introducing an initial compressive stress field in the rammed earth panel before the horizontal load is applied. In this regard, during the preparation stage of the test and before the upper timber beam is locked to the columns of the wooden frame, the vertical load is applied through the vertical jacks. In other terms, in this preliminary step, the top beam is free to slide down the columns and the compressive load applied by the two vertical jacks to the upper beam is transmitted directly to the panel without engaging the wooden columns. Once the preload phase is completed and the

50 kN vertical load is applied, the upper beam is connected to the columns, by inserting and tightening the bolts. At this stage, the mean compressive stress within the rammed earth panel is equal to 0.13 MPa. As observed in the previous section, this compressive stress is of the same order as that expected in ordinary two-storey residential buildings. The effect produced by different compressive stress levels on the reinforced panels should be investigated in further steps of the research.
The test set up for the shear load tests on the bare timber frames TF1 and TF2 is shown in Figure 5b. The same compressed air jacks “J1” and “J2” have been used. The tests on the two timber frames were carried out by controlling the jack head displacement.

During each test, the loads applied by the horizontal and vertical jacks are recorded. The displacement of the many points of interest on the timber frame and earth panel are recorded by means of 27 inductive displacement transducers (LVDT), whose positions are shown in Figure 6. In addition, the displacement of the horizontal jack traveling head is measured by the LVDT embedded in the jack itself (internal LVDT).
The values recorded during the test make it possible to quantitatively evaluate the global force-displacement response of the TREP element. Moreover, detailed information is collected concerning the deformed configuration of the frame, the actual stiffness of the connection between the timber beam and columns and the strain distribution in the rammed earth panel, with particular reference to its central part.

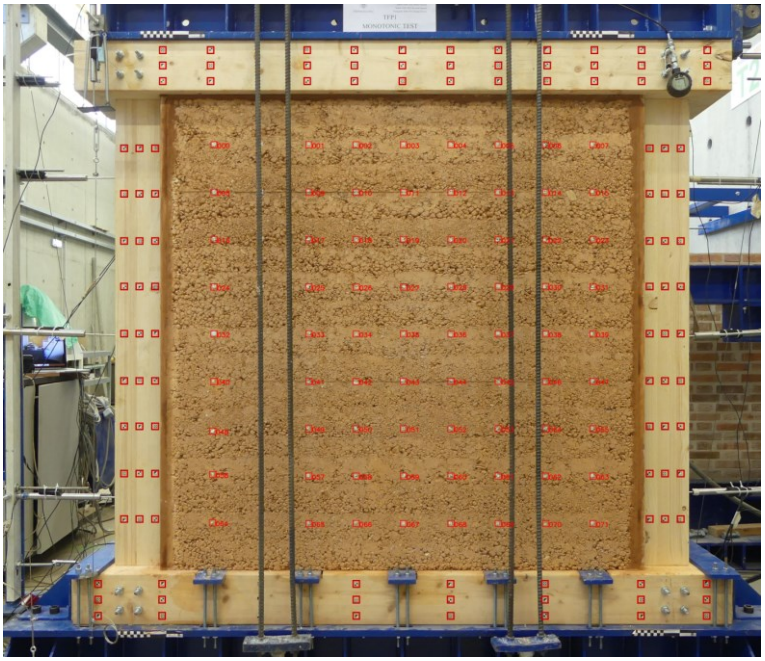

Figure 7. Markers used for displacement tracing of the timber frame and earth panel by DIC analysis.

Further information on the in-plane displacement field of the rammed earth panel and the timber frame is also obtained by exploiting the technique typically known as Digital Image Correlation (DIC). Based on well-established methods of photogrammetry, it is possible to follow the trajectory of specific points on the elements surface, identified by means of suitable markers applied to the same surfaces in the positions indicated in Figure 7. During each test, a frontal photo of the TREP element is shot every five seconds. The errors in the determination of the markers position due to the perspective and

curvature effects are digitally corrected by means of a script specifically written in Python by suitably adapting some functions available in the open-source OpenCV library. A ratio of 15 pixels/cm is chosen during the correction process. In this regard, since the faces of the different elements (*i.e.*, beams, columns, and panel) lie in different planes, although quite near, the TREP element has been ideally subdivided into five different regions in the DIC analysis: two for the beams (B1, B2), two for the columns (C1, C2) and one for the panel (RE). In this way the same pixel/cm ratio is assured in all parts of the TREP element, and the perspective effects are properly considered as well.

4. Test results

The main results obtained from the two shear-compression tests performed on the timber-framed rammed earth panels TREP1 and TREP2 are summarized in the following. As will be shown, the two tests provided very close results, and both highlight a more than satisfactory load capacity of the reinforced panels against horizontal actions.

4.1 Horizontal load-displacement curves for the bare timber frames

The TREP mechanical behavior is the result of the complex interaction between the rammed earth panel and the reinforcing timber frame. Hence, investigation of the bare frame response to the applied load is also relevant. In this regard, two monotonic shear load tests have been carried out on the bare timber frames TF1 and TF2; the horizontal load was imposed under displacement control. The first test has been interrupted when the lateral displacement reached 100 mm, and the unloading curve has been recorded. The test performed on the other timber frame TF2 has been pursued until the first signs of damage have been detected on the frame (Figure 8).

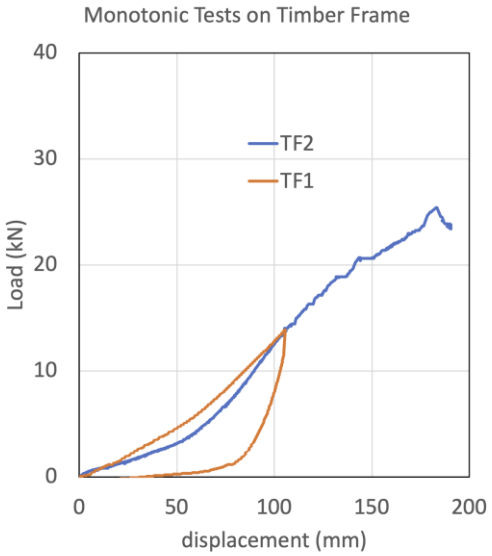

a)

b)

Figure 8. a) Load-displacement curves obtained from the monotonic tests performed on the timber frames; b) TF1 frame load test.

The two tests enable highlighting the low stiffness and strength of the bare frames. As it will be shown in the following section, the timber frame exhibited very low mechanical properties with respect to those of the timber reinforced rammed earth panels.

The TF2 load-displacement diagram can be ideally subdivided into three phases, each corresponding to a different mechanical response of the TF element. Phase 1, going from the origin up to 5 kN, is characterized by an increasing stiffness, probably due to the reduction of the play between the different parts composing the frame. Phase 2, roughly from 5 kN to 15-17 kN, shows an almost linear response of the frame. Lastly, phase 3 shows a progressive decrease in the stiffness that enables the frames to reach large displacements. When the frame reaches its maximum load capacity (25 kN) the displacement equals 200 mm. The stiffness within the linear range, for load values comprised between 5 to 15 kN, has been estimated as the slope of the linear regression line as 0.22 kN/mm.

4.2 TREP horizontal load-displacement curves

A key goal of the load test performed on the two timber-framed rammed earth panels TREP1 and TREP2 was to investigate the element's actual stiffness and load capacity under monotonically increasing horizontal loads. The diagrams plotted in Figure 9 show the load-displacement curves obtained from the two tests, considering the horizontal displacement recorded by the internal LVDT and the horizontal force exerted by the jack.

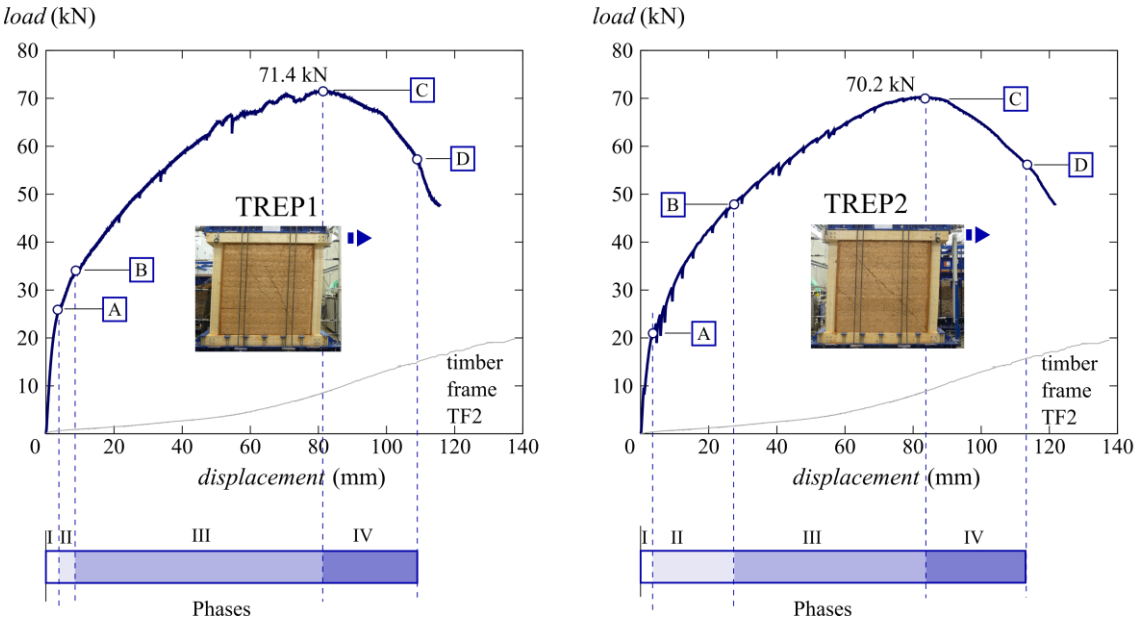

Figure 9: Load-displacement curves for the two tests.

The two diagrams are in very good agreement, some of their parts almost overlapping. Four points labelled A, B, C, D are highlighted on the diagram of each test. They ideally subdivide the load-displacement response curve into four phases (phase I - phase IV), each corresponding to a different mechanical response of the TREP element. In Figure 9 the displacement range of each phase is highlighted at the bottom of the diagram. More specifically, points A, B, C, D are linked to three indicators of the damage observed in the TREP elements, namely:

- relative vertical displacements between the upper beam and the columns,
- relative rotations between the upper beam and the columns,
- positive principal strain evaluated at the center of the panel.

The four points have been determined according to the following: (a) Point A corresponds to the first appearance of non-negligible values of at least one among the three damage indicators selected for the system; (b) Point B corresponds to the appearance of non-negligible values of all the three damage indicators selected for the system; (c) Point C marks the peak load registered during the test; (d) Point D corresponds to the ultimate lateral displacement (lateral load equal to 80 % of the maximum force).

Starting from the origin, both diagrams show a first part (I) which is practically linear. In this first phase, the stiffness of the TREP element under test is as high as 10 kN/mm in both tests. As the load increases the TREP stiffness progressively decreases, as expected. In this regard, the Phase II, from A to B, is characterized by the damage onset in both the frame joints and earth panel. More specifically, the onset of damage in the joints at the top was observed in correspondence to point A, while the onset of damage in the panel was observed in correspondence to point B, see Figures 10 and 11.
During the Phase III, from B to C, the element stiffness suffers a considerable decrease, going progressively to zero. The displacement range of the different phases is similar for both tests, however a smoother progressive decrease in the stiffness was observed for TREP2. As will be illustrated in the following, during the Phase III a marked diagonal crack developed in the rammed earth panel, clearly showing the establishment of a "strut-and-tie" resisting mechanism.
The maximum horizontal force, F_{max} recorded at point C during the tests was equal to 71.4 kN for the TREP1 and 70.2 kN for the TREP2. Since the mean vertical load imposed by both vertical jacks V_{avg} was found equal to 53.5 kN, the TREP elements can be considered able to withstand a horizontal load equal to 1.34 and 1.31 times the vertical one, respectively.
The displacement at the maximum horizontal load turned out to be equal to 81 mm and 83 mm for specimens TREP1 and TREP2, respectively. The test was pushed forward to the aim of investigating the post-peak response (Phase IV). This was accomplished by furtherly increasing the horizontal displacement until a 20 % decrease in the horizontal force was recorded. In agreement with the standard ISO 21581: 2010 [22], the ultimate displacement was identified with that corresponding to the 80 % of the maximum force (point "D" in Figure 9), which corresponded to 109 mm and 113 mm respectively. The load and drift values corresponding to the points A, B, C, D, highlighted on the load-displacement diagram are summed up in Table 3. The drift is assessed as the ratio between the horizontal displacement and the nominal heigh of the TREP element (1500 mm).

		A	**B**	**C**	**D**
TREP1	Load (kN)	26	34	71	57
	Drift (%)	0,2	0,6	5,4	7,3
TREP2	Load (kN)	21	48	70	56
	Drift (%)	0,2	1,8	5,5	7,5
Mean Values	Load (kN)	23,5	41	70,5	56,5
	Drift (%)	0,2	1,2	5,4	7,4

Table 3: summary of the results obtained from the shear-compression load test.

The obtained values of the horizontal bearing capacity are comparatively high. A comparison with the experimental results available in the literature is ~~will be~~ addressed in the Part II of the paper [4], ~~after~~ in which all the results obtained from ~~monotonic and~~ cyclic tests on the TREP specimens ~~will be~~ are also described. Here, as an anticipation it can be interesting to compare the results of the monotonic tests we performed with those

available in [23], which concern ~~and related to~~ unreinforced rammed earth panels of very similar shape. The results described in [23] are particularly relevant, as they concern panels having the same aspect ratio and thickness as those of the present work. In addition, the rammed earth compressive strength reported in [23] is twice as larger than that of the rammed earth used in our test. Hence, it is reasonable to assume that the load capacity of the unreinforced panel tested in [23] could be taken as an upper bound estimate for the load capacity of the rammed earth panels built for our tests.
In [23], the horizontal-to-vertical load ratio of the unreinforced panels is approximately equal to 0.36, which corresponds to barely 27 % of that of the TREP elements. Hence, the reinforcing timber frame seems to provide a substantial benefit enabling the development of a "strut-and-tie" resisting mechanism that effectively exploits the compressive strength of the rammed earth panel.
In Figure 9 the load-displacement curve for the bare timber frame TF2 is also plotted as a shaded gray line. It is straightforward to recognize that the timber frame stiffness and load capacity are much smaller than those of the whole TREP element. This comparison backs the conclusion that the good performance observed for the TREP elements are due to the beneficial confining effect that the timber frame exerts on the rammed earth panel rather than to the timber frame additional load capacity.

4.3 Summary of LVDTs' results

The data acquired by the LVDTs during the tests made possible to reconstruct the deformed configuration of the timber frame. Figure 10 shows the deformed configurations of the line of axis of the timber beams and column in both tests. The timber beams, firmly connected to the adjacent steel beams, can be assumed to remain straight with good approximation; the displacement of the columns axis was obtained by linearly interpolating the readings recorded by the LVDTs placed at half and quarter of their length (Figure 5b). For ease of representation, the displacements have been amplified by an order of magnitude. Figure 10 illustrates a small bending of the columns, thus confirming that, as the load increases, a "strut-and-tie" resisting mechanism is established and the timber frame is mainly subject to axial forces. Relative rotations between the top beam and columns are clearly recognizable as well.

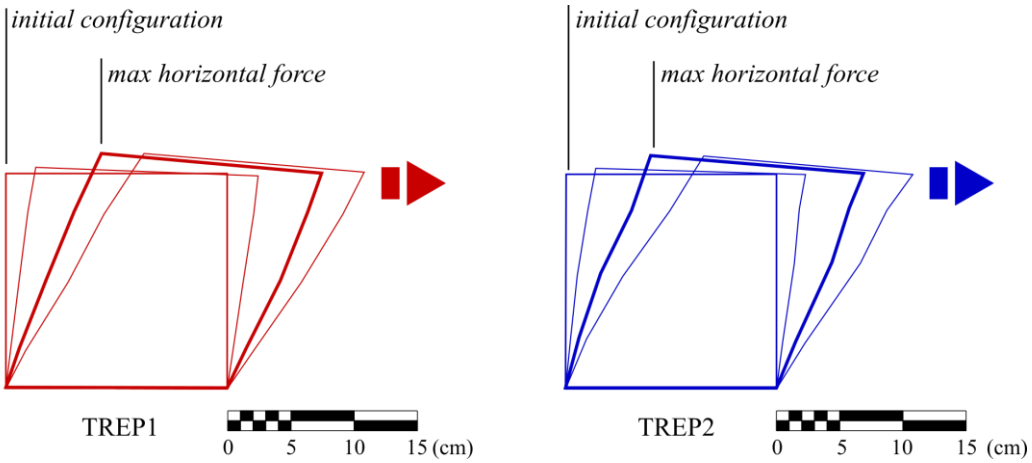

Figure 10: deformed configurations of the line of axis of the timber frame according to LVDTs (displacements magnified 10x): TREP1 test (on the left), TREP2 test (on the right).

The LVDTs near the frame joints (Figure 5d) made possible to have a closer look at the deformations in the neighborhood of the beam-to-column connections. In doing so, it is assumed that the upper timber beam undergoes a rigid motion composed of a translation and a rotation. This is a reasonable assumption as the timber beam is tightly connected to the top steel beam all over its length and it's free to rotate.

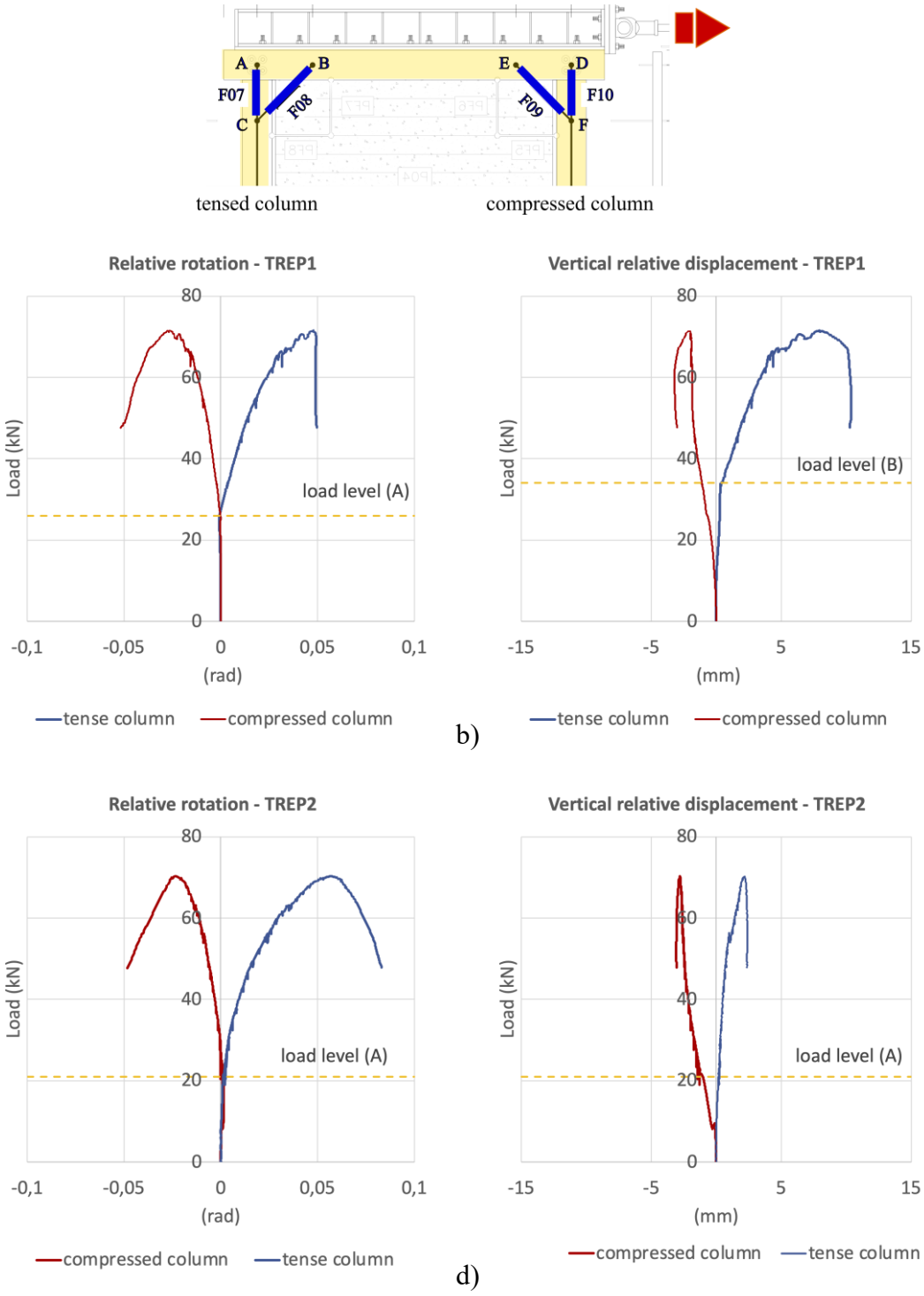

Figure 11: relative rotations and displacements between the top beam and the columns: TREP1 (figures a) and b)), TREP2 (figures c) and d)).

The data recorded by the transducers at each joint are used to the aim of assessing:

- the detachment between the top beam and column, Δv, by means of transducers F07 and F10;
- the relative rotation between the end parts of the top beam and column, $\Delta\theta$, by properly combining the readings provided by transducers F07, F08, F09 and F10 (see Table 4).

By indicating with Δ_i the readings from the LVDT labelled F_i in Figure 11, and by assuming that the displacements and rotations are sufficiently small, $\Delta\theta$ and Δv are assessed accordingly to Table 4 (l = 300 mm is the length of the vertical measurement base). The detachment is evaluated by neglecting the small elongation in the end part of the timber column.

	Compressed column	**Taut column**
Relative rotation Δθ	$\frac{\Delta_9\sqrt{2}}{l} - \frac{\Delta_{10}}{l}$	$\frac{\Delta_8\sqrt{2}}{l} - \frac{\Delta_7}{l}$
Beam-column detachment Δv	Δ_{10}	Δ_7

Table 4: beam-to-column relative rotation and detachment.

The diagrams of $\Delta\theta$ and Δv for the TREP1 and TREP2 tests are plotted in Figure 11. In the TREP1 test the rotations between the beam and columns begin when the load level reaches 25 kN (see the diagrams in Figures 11a and 11b). This is the first sign of the damage in the connections and, as already stated in the previous section, it has been recorded as point A on the load-displacement curve of the TREP1 plotted in Figure 9. As the horizontal load grows and becomes equal to 35 kN a clearly visible relative displacement, Δv, is recognizable in correspondence to the tensed column (Figure 11d). This load level, that marks the onset of the detachment, has been recorded as point B on the load-displacement curve of the TREP1. At the end of the test the detachment became as high as 10 mm. When the load reaches 65 kN, a sudden decrease in the stiffness is observed. It is worth observing that, instead, a much smaller relative displacement is observed in the compressed column.

When the horizontal load is low (*i.e.*, during the Phase I and Phase II of Figure 9) the connections between beam and columns effectively constraint the relative rotations; for larger load levels (Phase III and Phase IV), a "strut-and-tie" resisting mechanism is established and relative rotations between beam and columns appear.

The strong difference observed in the diagrams of the relative displacement for the tensed and the compressed column (Figure 11b) clearly display a different damage process undergone by the corresponding connection. More specifically, in the tensed column, as the traction in the column increases, it is reasonable to imagine that the bearing stress between the screws and the wood could become so high as to cause failure in the material. The connection begins to damage significantly starting from about 50 % of the maximum load. This finding confirms that the damage in the joints plays a relevant role in the stiffness decay of the overall element observed in Phase III.

Similar results were also obtained from the TREP2 test concerning the rotations between the beam and columns, which begin when the load level reaches 21 kN (Figure 11c). Smaller vertical displacements have been observed in this case at the top of the columns (Figure 11d). Some adjustment of the compressed joint occurs since the beginning of the test.

The LVDTs at the centre of the earth panel (Figure 4d) enabled assessing the strain state. Six LVDTs (P01 - P06, shown in Figure 12) have been arranged in the central area of the rammed earth panel to evaluate the average state of strain in that area. Simple geometric considerations enable expressing the mean value of the strain components in terms of the LVDTs' readings. Moreover, since three strain components are unknown, while six quantities have been measured, the redundancy in the data enables searching for the optimum strain values that best fit the experimental measurements through the method of least squares.

More specifically, Δ_1 and l_1 indicate the readings and the length of the vertical measurement base of the LVDT labelled P01, with Δ_2 and l_2 those of P02 and so on; moreover let (x, y) be a cartesian reference system, with x horizontal, let (a_1, b_1) be the components of the unit vector along the direction of P01, (a_2, b_2) that of P02 and so on. The strain components ε_x, ε_y, γ_{xy} are determined by setting:

$$\sum_{i=1}^{6}\left(\varepsilon_x a_i^2 + \varepsilon_y b_i^2 + \gamma_{xy} a_i b_i - \frac{\Delta_i}{l_i}\right)^2 = min \tag{1}$$

Once the cartesian components of strain are determined, the principal strain values ε_I and ε_{II} are assessed; the results are shown in Figure 11.

It is interesting to observe that non negligible deformations in the panel are observable when the load exceeds 35 kN for TREP1 test and 45 kN for TREP2 test. These threshold values correspond to point "B" in the overall load-displacement diagrams (Figure 9). This result allows to reckon that during the Phase I and Phase II, *i.e.*, in the first phases of the TREP mechanical response, the whole earth panel is involved in the resisting mechanism. On the contrary, when the load exceeds the above-stated threshold values, and the TREP element enters the Phase III of its mechanical response, a diagonal compression field starts developing in the central area of the panel, while the stresses progressively decrease in the off-diagonal parts of the panel.

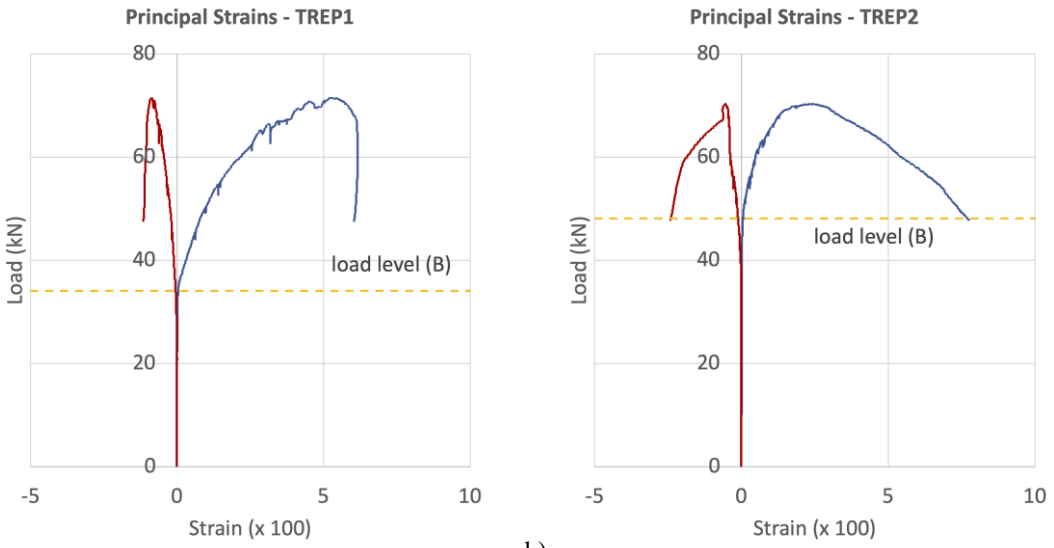

a) b)

Figure 12: principal strain values at panel center: a) TREP1 test; b) TREP2 test.

Starting from the onset of the Phase III, both tests display large increments in the positive strains at the center of the panel, while the slope of the negative strain marks a sharp change. As expected, the negative strains are considerably lower (in absolute value) than the positive ones. The apparent large positive strains are likely due to the progressive growth of the diagonal cracking pattern clearly observable in the earth panel, as described in the preceding section. Therefore, it is reasonable to assume that the stiffness decay of the overall element observed in Phase III is produced by the combined effect of the damage in the frame joints and the development of the diagonal compressed strut in the earth panel. In this regard, by considering that the rammed earth elastic modulus has been estimated as high as 100 MPa, and that the maximum compressive strain, in absolute value, is equal to about 0.009, the order of the ultimate compressive stress in the panel can be estimated as 100 x 0.009 = 0.9 MPa.

4.4 Digital Image Correlation

During the TREP tests, a series of photographic shots were taken of the panel and timber elements. All the frames have been processed using the standard methods of the Digital Image Correlation (DIC), which have been mentioned at the end of Section 3. In this way, the analysis made it possible to follow the trajectories of a given set of points identified before the test on the surface of both the panel and the timber elements.

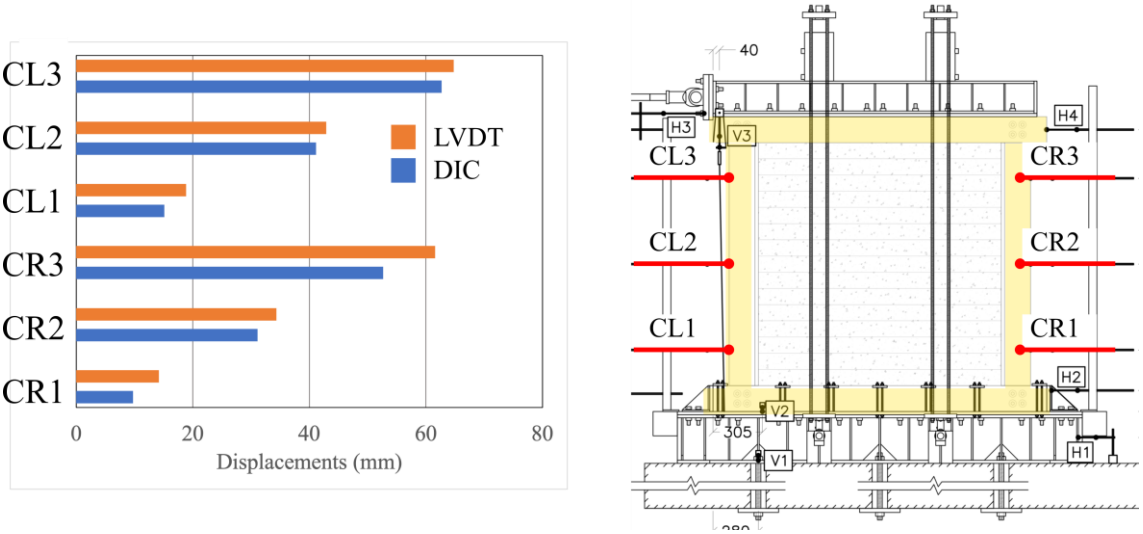

Figure 13: Comparison between DIC (blue) and LVDT (orange) displacements recorded on the columns of TREP1 specimen test at maximum horizontal load.

The displacements evaluated through DIC were validated by comparing them with those measured directly by the LVDTs. The result of the comparison with the transducers on the timber frame columns during the TREP1 test is shown in Figure 13. The graphs show the horizontal displacements of three points along the columns obtained by the LVDTs and by DIC at reaching of the maximum load during the test. The mean error is equal to 17 %. The agreement between the two set of measurements can be considered more than acceptable for the purpose.

As for the rammed earth panel, the displacements of 9 x 8 = 72 points on the panel surface were observed through DIC, in correspondence to the nodes of a 15 cm x 15 cm square mesh grid. By post-processing the recorded data it has been possible to estimate the strain field corresponding to each analysed frame. Deformations were evaluated using the well-known central finite differences approximating formula of the first derivatives. An

example of the results obtained by this way, Figure 14 shows a colour map of the principal positive strain in the panel assessed by means of the DIC data recorded at the peak horizontal load. The strain magnitude is proportional to the colour intensity, according to the legend on the right of the graph. The higher values are gathered around the diagonal of the panel, consistently with the appearance of the diagonal cracks that were clearly observed in the same area during the test.

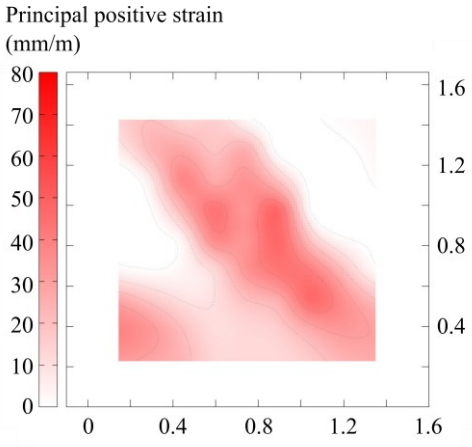

Figure 14: Positive principal strains within the TREP1 panel for F = 71.5 kN (maximum horizontal load)

5. Damage survey

5.1 Damage survey in the TF elements

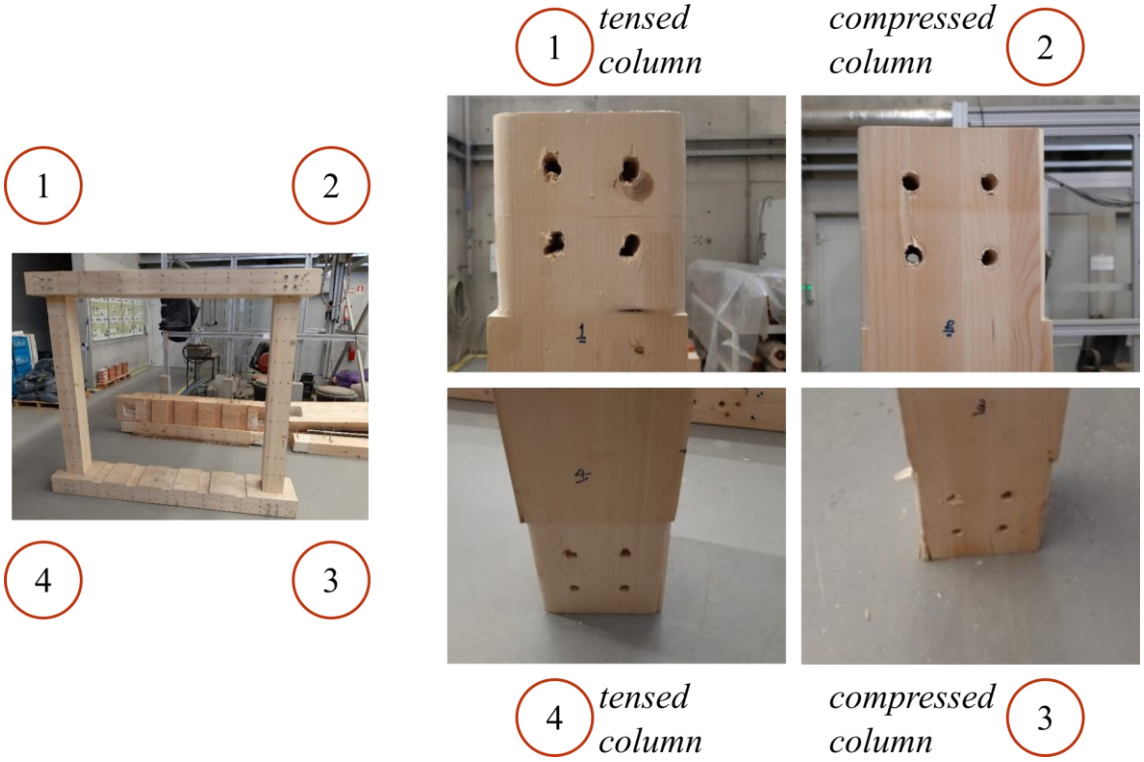

Figure 15: TF2 test – Highlight of the damage in the joint holes of the timber columns.

The damage survey performed after the loading test on the bare timber frame TF2 enabled recognizing the damage level attained in the joints (Figure 15).
As expected, the joints in the bare frames turn out to be more severely damaged with respect to their counterparts embedded in the TREP elements. Figure 15 shows large ovalization of the bolt holes due to high bearing stresses in the wood.

5.2 Damage survey in the TREP elements

The condition after the test of the two TREP elements are shown in Figure 16 and Figure 17. A visual inspection enabled recognizing: (a) severe diagonal cracking in the earth panel (D1); (b) partial detachment between the rammed earth layers and between the panel and surrounding frame (D2); (c) crushing and out-of-plane expulsion of the soil (D3).

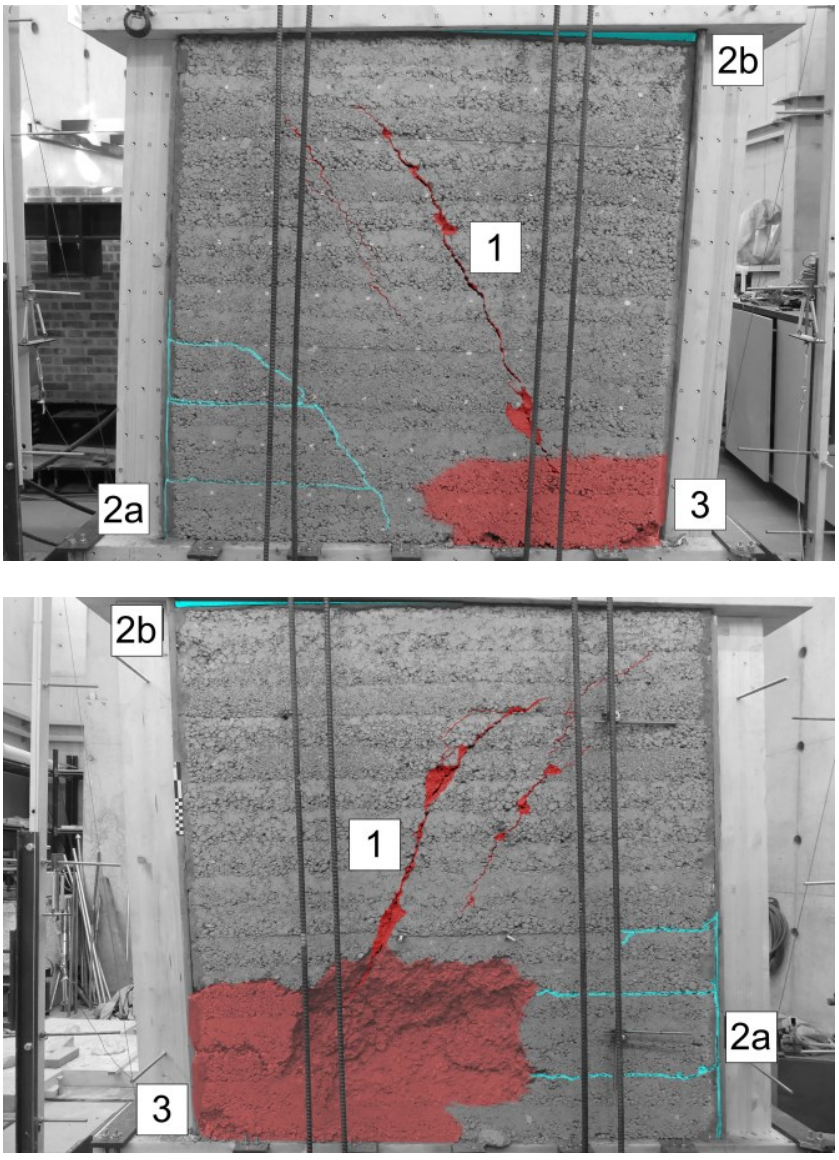

a)

b)

Figure 16: Highlight of the damage in the TREP1 rammed earth panel; *a*) front view, *b*) rear view.

The diagonal cracking pattern in the earth panel (D1) is highlighted as red lines in Figure 14 and Figure 15. In the TREP1 test cracks (1) were observed starting from a horizontal force of 40 kN. In the TREP2 test the first crack (1a) appeared in the lower left corner when the horizontal force was close to 35 kN, while the central ones (1b) appeared at 50 kN. The position and inclination of these cracks are consistent with the formation in the earth panel of a resisting mechanism, as expected, characterized by a diagonal compressed part (strut), analogous to that usually observed in framed masonry structures. As for the detachment between the rammed earth layers and between the panel and surrounding frame (D2), the relative rotations and detachment between the top beam and columns enabled the development of a progressive detachment between the panel and surrounding frame, as well as between the rammed earth layers. The detached portions are highlighted in the images as blue lines. In the TREP1 test the detachments became visible between the layers in the lower portion (2a) when the load reached 54 kN; the detachments along a portion of the interface between the frame upper beam and the panel (2b) were observed when the load reached 62 kN. In the TREP2 test the first detachments between the lateral sides of the earth panel and the timber frame (1a) were observed for lower load values, equal to about 35 kN; further detachments between the upper side of the panel and the frame appeared at some 64 kN.

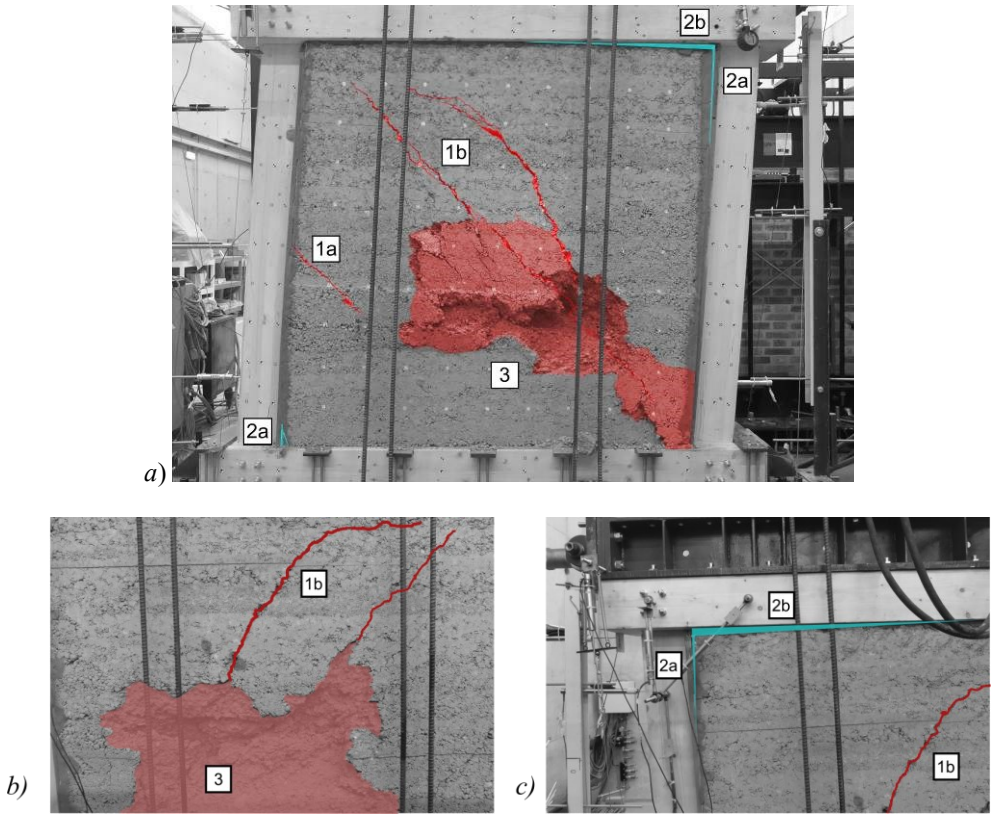

Figure 17: Highlight of the damage in the rammed earth panel of TREP2; *a*) front view, *b*) and *c*) rear view.

The portions of the earth panels that undergone crushing and out-of-plane expulsion phenomena (D2) are highlighted in red in the images. The expulsion is produced by a local instability mechanism promoted by the progressively increasing compressive

stresses. In both tests, the expulsion of a consistent amount of material at the bottom of the panel occurred at 70 kN.
The detachments between the panel and frame began to be observed for loads a bit higher than those that mark the beginning of damage in the frame connections. In other words, damage in the frame connections seems to start before the detachment between the panel and the frame. As the load increases the two phenomena progressively develop, both contributing to the nonlinear trend of the observed response curve of the TREP elements. The collapse of the whole TREP element is reached when the last damage mode, in order of appearance, is observed in the earth panel, *i.e.*, the expulsion of the most compressed portions of the panel.

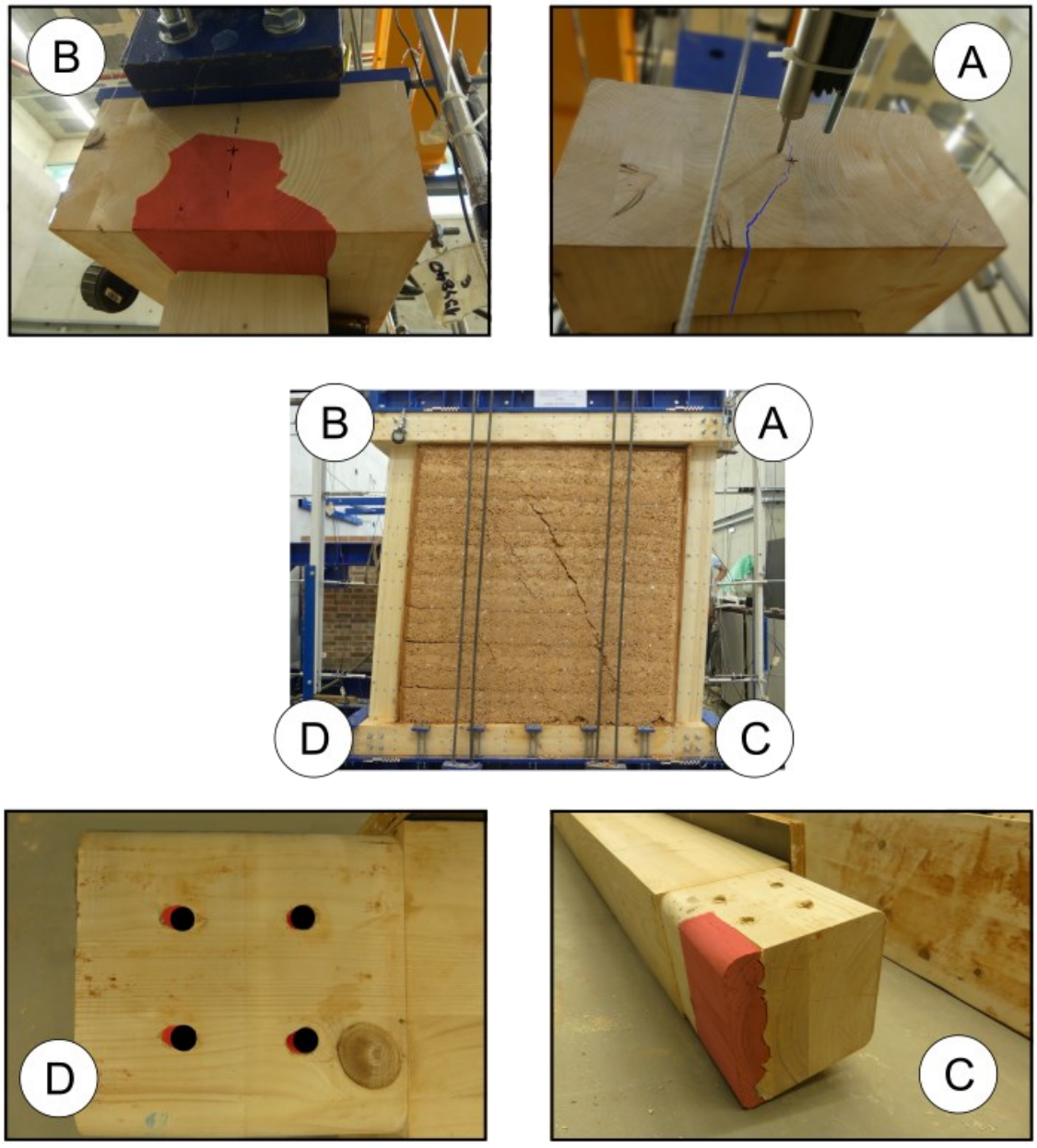

Figure 18: damage in the joints frame of TREP1.

At the end of the two loading tests, the elements were carefully dismantled to enable verifying the presence and extent of damage in the various parts.
The damages and failure observed in the timber elements are mainly located in correspondence to the frame joints. As far as TREP1 is concerned, the damages detected at the end of the test are shown in the photos collected in Figure 18. Joints B and C, that is, those at the ends of the compressed strut within the earth panel, revealed a much more pronounced damage level when compared to the other two joints, D and A, the latter being practically free of signs of damage. The damaged portions are highlighted in red in Figure 18. The survey clearly shows that damage in the joints plays a crucial role in the structural response of the TREP elements. Yet, further tests will be needed to understand how the different failure modes unfold by varying timber elements dimension and strength.

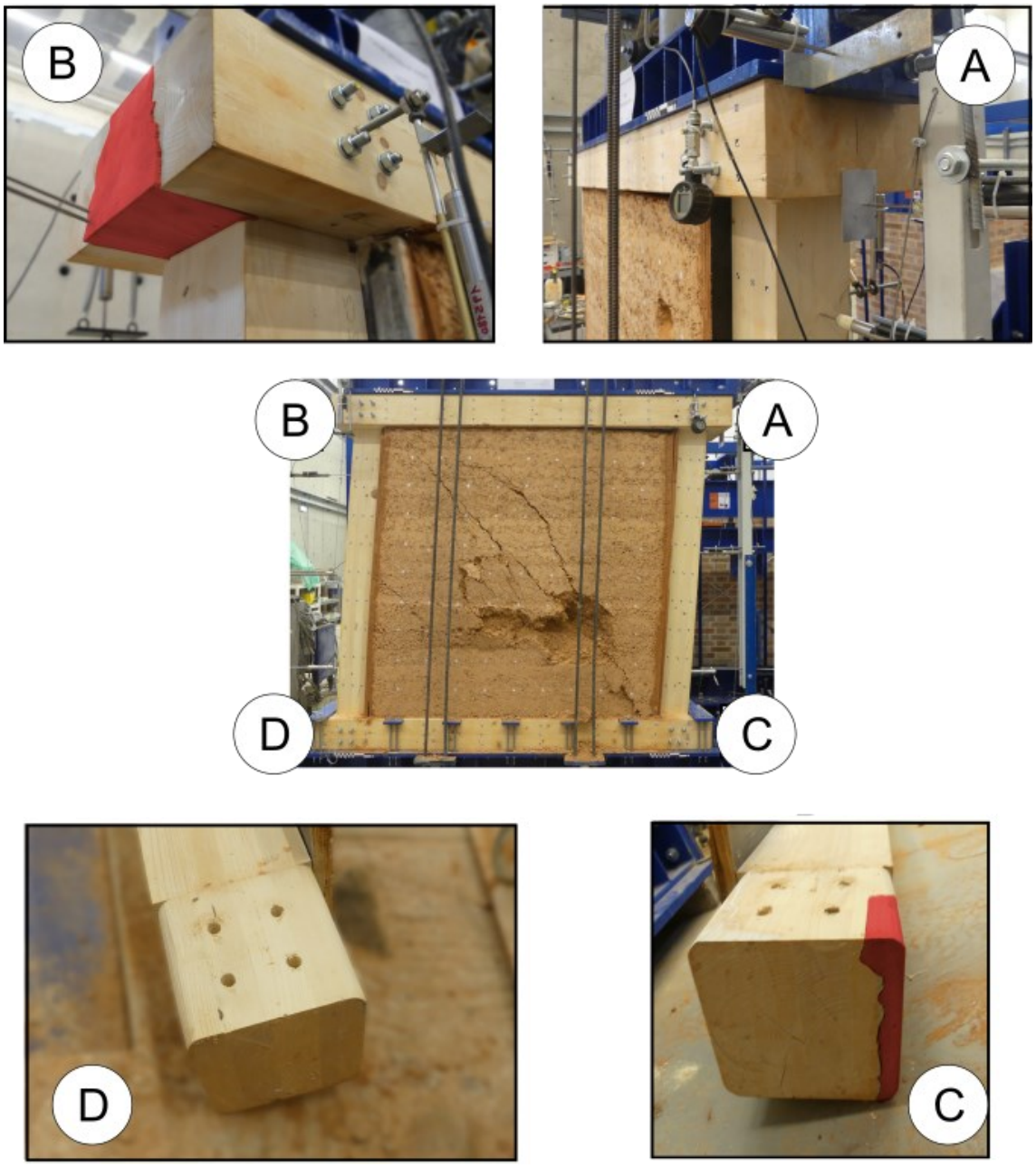

Figure 19: damage in the joints frame of TREP2.

The contact pressure between beam and column at joint B led to the shear failure of the upper beam external portion (Figure 18B). Similarly, at joint C, the partial detachment is observed of the lateral portion at the column bottom outside the bolting area (Figure 18C). The holes at joint D shown clear signs of the high bearing stress levels (Figure 18D). In this regard it is worth observing that the corresponding bolts shown evident permanent deformations (yielding) at the end of the test. Quite similar observations can also be made for TREP2 test (Figure 19). In this case, however, the damage due to the bearing stresses at joint D was much less marked.

6. Conclusions

As well known, rammed earth walls show comparatively good performances with respect to vertical loads, while their stiffness and strength against horizontal loads are in many cases unsatisfactory. To provide rammed earth panels with some additional strength and stiffness against horizontal actions, a reinforcing timber frame has been connected to the panel, thus making up a composite element indicated as “Timber Framed Rammed Earth Panel” (TREP).

Valuable indications about the TREP stiffness and load bearing capacity have been obtained by a first set of experimental studies that has been expressively set up and performed. The experiments focused on the TREP in-plane static behaviour, by performing a series of in-plane shear-compression tests, both monotonic and cyclic. The monotonic tests have been illustrated in the present paper (part I); the cyclic tests are addressed in the companion paper (part II). As per the monotonic tests, two elements have been built and tested until collapse under in-plane shear-compression loading condition, as described above.

The load-displacement curves obtained from the two tests are in very good agreement. In both cases, a four-phases decomposition of the global structural response can be clearly recognized. As per the horizontal load capacity, the TREP elements exhibited a horizontal-to-vertical load ratio equal to some 1.3, which roughly corresponds to three or four times that of unreinforced panels having the same aspect ratio and thickness. The reinforcing timber frame seems to provide a substantial benefit enabling the development of a “strut-and-tie” resisting mechanism that effectively exploits the compressive strength of the rammed earth panel. A ductile failure mode has been observed and an ultimate horizontal drift of 7 % has been reached by both the TREP elements.

During both tests, the data collected from the LVDTs as well as those obtained by suitably adapting the Digital Image Correlation technique enabled following the deformed configuration of the timber frame, the actual rotations in correspondence to the frame joints and the strain level in the earth panel. A very good agreement has been observed between the results obtained by different methods. The damage survey performed after the tests enabled highlighting the damage modes involved, confirming that the damage in the joints plays a crucial role in the structural response of the TREP elements.

The present paper addressed the experimental results obtained from a first series of in-plane loading tests. A mechanical model for interpreting the results obtained from monotonic and cyclic loading tests will be illustrated in a forthcoming paper. Further steps of the research will address the system mechanical response to out-of-plane actions.

Acknowledgments
The authors wish to thank Claudio Tirabasso, formerly a doctoral student at the University of Pisa, for his valuable help in designing, planning and executing the experimental tests.

References
[1] H. Schroeder, (2016). Sustainable Buildings with Earth, Springer International Publishing Switzerland.
[2] Langenbach R (2007). From "Opus Craticium" to the "Chicago Frame": Earthquake-Resistant Traditional Construction, International Journal of Architectural Heritage 1(1): 29-59.
[3] Vieux-Champagne F, Sieffert Y, Grange S, Polastri A, Ceccotti A and Daudeville L (2014). Experimental analysis of seismic resistance of timber-framed structures with stones and earth infill, Engineering Structures 69: 102-115.
[4] V. Baleca, R. Barsotti, S. Bennati, D. Oliveira (2023). Experimental investigation of in-plane loaded timber-framed rammed earth panels. Part II: cyclic shear-compression tests, Structures.
[5] Maniatidis V., Walker P. (2008). Structural Capacity of Rammed Earth in Compression, Journal of Materials in Civil Engineering, 20 (3): 230–238.
[6] Kariyawasam K.K.G.K.D., Jayasinghe C. (2016). Cement stabilized rammed earth as a sustainable construction material, Construction and Building Materials, 105: 519–527.
[7] Silva R.A., Oliveira D.V., Miranda T., Cristelo N., Escobar M.C., Soares E. (2013). Rammed earth construction with granitic residual soils: The case study of northern Portugal, Construction and Building Materials, 47: 181–191.
[8] Bui T.T., Bui Q.-B., Limam A., Maximilien S. (2014). Failure of rammed earth walls: From observations to quantifications, Construction and Building Materials, 51: 295–302
[9] Romanazzi, A., Oliveira, D.V., Silva, R.A., Barontini, A., Mendes, N. (2022). Performance of rammed earth subjected to in-plane cyclic displacement, Materials and Structures, 55, 54(2022), 2022
[10] Kai Liu K., Wang M., Wang Y. (2015). Seismic retrofitting of rural rammed earth buildings using externally bonded fibers, Construction and Building Materials, 100: 91–101.
[11] Fagone M., Kloft H., Loccarini F., Ranocchiai G. (2019). Jute fabric as a reinforcement for rammed earth structures, Composites Part B, 175: 107064.
[12] NZS 4297, Engineering Design of Earth Buildings, Wellington: New Zealand Standard, 1998.
[13] Standards Australia, The Australian Earth Building Handbook, Australia Standards, Sydney, 1998.
[14] G. Tampone (1996). The restoration of timber structures (in Italian). Milan, Libreria Tecnica Hoepli.
[15] D. D'Ayala, P. Tsai (2008). Seismic vulnerability of historic Dieh–Dou timber structures in Taiwan. Engineering Structures, 30: 2101–2113.
[16] J. Mascarenhas (2004). Constructive systems – V (in Portuguese). Livros Horizonte, Lisbon.
[17] R. Langenbach (2009) Don't tear it down! Preserving the earthquake resistant vernacular architecture of Kashmir. UNESCO, New Delhi

[18] Historical Earthquake-Resistant Timber Framing in the Mediterranean Area, HEaRT 2015. Eds. H. Cruz, J. S. Machado, A. C. Costa, P. X. Candeias, N. Ruggieri, J. M. Catarino. Springer, 2016.
[19] Asociacion Colombiana de Ingenieria Sismica (2004). Manual para la rehabilitacion de viviendas construidas en adobe y tapia pisada.
[20] Sassu M, Romanazzi A, Giresini L, Franco W, Ferraresi C, Quaglia G, Orefice E (2018). Production procedures and mechanical behaviour of interlocking stabilized compressed earth blocks (ISCEBs) manufactured using float ram 1.0 press, Engineering Solid Mechanics, 6 (2): 89-104.
[21] Houben H, Guillad H (1994). Earth Construction: A comprehensive guide. Intermediate Technology Publications, Michigan.
[22] ISO 21581:2010, Timber structures - Static and cyclic lateral load test methods for shear walls, International Organization for Standardization, Switzerland, 2010
[23] El-Nabouch R, Bui QB, Plé O, Perrotin P (2017). Assessing the in-plane seismic performance of rammed earth walls by using horizontal loading tests, Engineering Structures 145: 153-161.